

Batched First-Order Methods for Parallel LP Solving in MIP

Nicolas Blin¹, Stefano Gualandi², Christopher Maes¹, Andrea Lodi³, Bartolomeo Stellato⁴

NVIDIA¹

*Department of Mathematics, University of Pavia*²

*Jacobs Technion-Cornell Institute, Cornell Tech*³

*Department of Operations Research and Financial Engineering, Princeton University*⁴

January 30, 2026

Abstract

We present a batched first-order method for solving multiple linear programs in parallel on GPUs. Our approach extends the primal-dual hybrid gradient algorithm to efficiently solve batches of related linear programming problems that arise in mixed-integer programming techniques such as strong branching and bound tightening. By leveraging matrix-matrix operations instead of repeated matrix-vector operations, we obtain significant computational advantages on GPU architectures. We demonstrate the effectiveness of our approach on various case studies and identify the problem sizes where first-order methods outperform traditional simplex-based solvers depending on the computational environment one can use. This is a significant step for the design and development of integer programming algorithms tightly exploiting GPU capabilities where we argue that some specific operations should be allocated to GPUs and performed in full instead of using light-weight heuristic approaches on CPUs.

Keywords: Mixed-Integer Linear Programming, First-order method, Parallel computing, GPU architectures.

1 Introduction

First-order methods for solving linear programming (LP) problems have recently been rediscovered for the (approximate) solution of very large instances. This is due to the fact that first-order methods are a natural choice for parallelization, which in turn is the relevant characteristic to look into for exploiting GPUs.

Although there has been significant progress in solving LPs with first-order methods starting from the first GPU implementations of operator-splitting solvers based on the alternating direction method of multipliers (ADMM), such as the SCS solver O’Donoghue et al. [2016], O’Donoghue [2021] and the OSQP solver Stellato et al. [2020], Schubiger et al. [2020] and, more recently, the primal-dual hybrid gradient (PDHG) algorithm Chambolle and Pock [2011] implementation in the PDLP solver Applegate et al. [2021, 2023], Lu and Yang [2025], the target of this research area has been (so far) solving extremely large LPs and there is some skepticism that this technology can be applied in mixed-integer programming (MIP) Rothberg [2024]. This is due to the fact that interior point algorithms are also very effective and parallelizable (so, solving the LP relaxation of any MIP is somehow doable) and the simplex method seems unbeatable in its ability of warm-starting in the presence of a small modification of the solution space due to the change of a variable bound or the addition of a round of cuts.

The GPU use in MIP has been also limited by the technological burden of moving large amounts of data from CPUs (where the computation has been run traditionally) to GPUs and vice versa. This difficulty has been observed for example in the context of the use of machine learning (ML) models to augment branch-and-bound methods Scavuzzo et al. [2024]. Indeed, some significant success has been already obtained (see,

e.g., Bonami et al. [2022], Berthold et al. [2025]), but the CPU vs GPU interaction has slowed down the adoption of ML models using neural networks (NN) representations, especially when those models need to be run at each node of the branch-and-bound tree like, for example, for variable selection in branching Gasse et al. [2019], Gupta et al. [2020].

In other words, it is possible that an effective GPUs exploitation in MIP – besides the technological improvement in GPU memory – requires rethinking the branch and bound itself, potentially abandoning some of its foundational certainties (the simplex method) and removing its computational work limits.

Along this rethinking path, the current paper shows that one GPU benefit for MIP is on exploiting the parallelization power to execute in full on GPUs chunks of the computation that, traditionally, are performed by clever heuristics that guarantee good approximations and limit the computational load. This is the case of strong branching and optimization-based bound tightening that involve the solution of batches of LPs with minimal differences (variable bounds). State-of-the-art implementations of batched LP solutions arise in differentiable optimization, where problems are structured as neural network layers Agrawal et al. [2019], Lu et al. [2024], Besançon et al. [2023], and primarily use basic vectorization operations (*e.g.*, `vmap`). These methods do not fully exploit the parallelism of GPU-based matrix operations and require data duplication across batch instances since many solvers lack full thread safety for parallel instance solving.

In this paper, we propose a fully parallelizable first-order method directly designed to solve batches of LPs all at once on GPUs, overcoming limitations of existing batch approaches. In the case of strong branching, this allows a precise initialization of pseudocosts (the capillary information MIP solvers use for guiding branching) in only a few rounds of memory communication, thus gaining quality without paying a high price for GPU vs CPU interaction.

The remainder of the paper is organized as follows. In Section 2, we review the relevant literature concerning first-order methods for LPs and their GPU implementations. In Section 3, we present the way we formulate an LP so as to be amenable to the first-order algorithm described in Section 4. In Section 5, we discuss our contribution in solving batches of LPs by first-order methods. In Section 6, we present our computational experiments with our implementation of BATCHLP to perform strong branching and OBBT on standard benchmarks from the literature. Finally, in Section 7, we draw some conclusions.

2 Literature review

The first effective first-order method for LP is the PDLP algorithm Applegate et al. [2021, 2023]. PDLP applies the primal-dual hybrid gradient (PDHG) method, see Chambolle and Pock [2011], and uses restarting and averaging to accelerate it. Several other enhancements were included in PDLP such as adaptive step-size (see also Chambolle et al. [2024]) and problem scaling.

Building on PDLP, the Halpern Peaceman-Rachford (HPR) method takes a weighted average between the current PDHG iterate and an initial point Lu and Yang [2024]. The initial point is updated when certain restart conditions are met. This leads to an algorithm called restarted Halpern PDHG (rHPDHG). A similar restarted Halpern algorithm is developed in Chen et al. [2025] with a relaxation step that results in a longer step size. Inspired by Chen et al. [2025], an extension is considered in Lu and Yang [2024], called reflected restarted Halpern PDHG (r^2 HPDHG), where the Halpern iteration is performed on the reflection of the PDHG operator instead of the operator itself. Finally, the extension of rHPDHG to conic LP is presented in Xiong and Freund [2024].

In terms of successive improvements of the PDLP algorithm, a geometric interpretation of the PDLP behavior is presented in Liu and Lu [2024] and based on such interpretation a new crossover algorithm is designed to recover a vertex solution for an LP. A key role in this type of algorithms is played by infeasibility detection, *i.e.*, recognizing infeasible subproblems, so as to avoid useless iterations. This is extensively explored in Applegate et al. [2024], Banjac et al. [2019].

The idea of extending a first-order method to solve batches of linear programs on the GPU for strong branching was first introduced in Nair et al. [2020]. The goal and methodology in Nair et al. [2020] are fundamentally different from our proposal because the GPU implementation of strong branching is used to collect data for training an ML model at the branching task, *i.e.*, to approximate strong branching. Instead,

in this paper, we propose to use GPUs to do strong branching, not approximate it, for a certain number of iterations that allow to initialize pseudocosts. Besides the different motivation, the way in which the GPUs are used for strong branching is very different. In [Nair et al. \[2020\]](#), the batches of LPs are solved by a modification of ADMM, and in a setting where instead of branching on fractional variables the MIP algorithm branches on all variables. Finally, the assessment of the speed-up with respect to traditional CPU implementations does not consider the fact that each LP can be solved by starting from the optimal basis of the simplex method, so generally doing only very few pivots to converge. This leads to an overestimation of the speed-up while our methodology assesses it very carefully in different benchmark settings, see Section 6.

3 Problem formulation

Consider a linear optimization problem in the primal-dual form

$$\begin{array}{ll} \min & c^T x \\ \text{s.t.} & \begin{array}{ll} \max & -\phi_{[\underline{x}, \bar{x}]}(r) - \phi_{[l, u]}(y) \\ l \leq Ax \leq u, & \text{s.t.} \quad c + A^T y + r = 0 \\ \underline{x} \leq x \leq \bar{x}, & y \in B_{[l, u]}, \quad r \in B_{[\underline{x}, \bar{x}]}, \end{array} \end{array} \quad (1)$$

where the decision variables are $x \in \mathbf{R}^n$, and the coefficients of the linear objective function are $c \in \mathbf{R}^n$. The constraints are defined by matrix $A \in \mathbf{R}^{m \times n}$ and vectors l, u, \underline{x} , and \bar{x} , with $l_i, \underline{x}_i \in \{-\infty\} \cup \mathbf{R}$ and $u_i, \bar{x}_i \in \mathbf{R} \cup \{+\infty\}$. We represent equality constraints as $l_i = u_i$ and variable fixings as $\underline{x}_i = \bar{x}_i$. We define the dual variables for the inequality constraints as $y \in \mathbf{R}^m$ and for variable bounds as $r \in \mathbf{R}^n$. The set B represents the barrier cone of a hyperrectangle, *i.e.*, $B_{[a, b]} = \{v \mid v_i \geq 0 \text{ if } a_i = -\infty; v_i \leq 0 \text{ if } b_i = \infty; v_i \in \mathbf{R} \text{ otherwise}\}$. Function ϕ represents the support function of a hyperrectangle, *i.e.*, $\phi_{[a, b]}(v) = \sup_{z \in [a, b]} v^T z = b^T v_+ + a^T v_-$, where $v_+ = \max\{v, 0\}$ and $v_- = \min\{v, 0\}$.

To derive our algorithm, we reformulate (1) as the following saddle-point problem

$$\max_y \min_{\underline{x} \leq x \leq \bar{x}} c^T x + y^T A x - \phi_{[l, u]}(y). \quad (2)$$

4 Primal-dual hybrid gradient to solve a single instance

We apply the primal-dual hybrid gradient method (PDHG) [Chambolle and Pock \[2011\]](#) with reflected Halpern iterations [Halpern \[1967\]](#), [Lu and Yang \[2024\]](#), [Lu et al. \[2025\]](#) to solve problem (1). The iterations in terms of the primal-dual pair $z^k = (x^k, y^k) \in \mathbf{R}^{n+m}$ consist of

$$z^{k+1} = \frac{k+1}{k+2} (2T(z^k) - z^k) + \frac{1}{k+2} z^0, \quad (3)$$

with the main operator T being defined as

$$T(z^k) = \left\{ (x, y) \left| \begin{array}{l} x = \Pi_{[\underline{x}, \bar{x}]} (x^k - \tau(c + A^T y^k)) \\ y = y^k + \sigma A(2x - x^k) - \sigma \Pi_{[l, u]}(\sigma^{-1} y^k + A(2x - x^k)) \end{array} \right. \right\}.$$

Here, z^0 is the initial iterate used in the Halpern iterations as the anchor point. Moreover, $\Pi_{[a, b]}$ is the Euclidean projection onto a hypercube defined as the elementwise operation $\Pi_{[a, b]}(v) = \max\{\min\{v, b\}, a\}$. The primal and dual step-sizes are τ and σ , respectively. As commonly done in PDHG [Applegate et al. \[2021\]](#), we parametrize the step sizes as $\tau = \eta/w$ and $\sigma = \eta w$, where we refer to η as the step size and w as the primal weight.

Restarts. Similarly to [Lu et al. \[2025\]](#), we apply an adaptive restart scheme based on the fixed-point residual progress of the non-reflected iterates. More specifically, we define the fixed-point residual metric

$$r(z) = \|T(z) - z\|_M, \text{ with } M = \begin{bmatrix} (w/\eta)I & A^T \\ A & (1/(\eta w))I \end{bmatrix}. \quad (4)$$

To restart, we partition the iterations in two loops, an outer loop indexed by n and an inner loop indexed by k , with corresponding iterates $z^{n,k}$. The algorithm repeats iteration (3) until one of the following restart conditions is met:

- sufficient decay: $r(z^{n,k}) \leq \beta_s r(z^{n,0})$,
- necessary decay and no inner progress: $r(z^{n,k}) \leq \beta_n r(z^{n,0})$ and $r(z^{n,k}) > r(z^{n,k-1})$, and
- iteration limit: $k > \beta_a K$, with K being the total number of iterations.

In this case, the anchor point z^0 is set to the current iterate.

Step-size and primal weight. We adopt the constant step-size from [Lu et al. \[2025\]](#), where $\eta = 0.998/\|A\|_2$ and the exponential smoothing technique to update the primal weight w [Applegate et al. \[2025\]](#). Specifically, whenever $d^n = \|x^{n+1,0} - x^{n,0}\|/\|y^{n+1,0} - y^{n,0}\|$ is finite at every outer loop iteration, we update $w^{n+1} = \exp(\theta \log(d^n) + (1 - \theta) \log(w^n))$.

Stopping criteria. This algorithm, including restarts, has been analyzed in [Lu and Yang \[2024\]](#) and shown to converge at a linear rate. We terminate the algorithm if the following optimality conditions are satisfied:

$$\begin{aligned} |c^T x^k + \phi_{[\underline{x}, \bar{x}]}(r^k) + \phi_{[l, u]}(y^k)| &\leq \epsilon(1 + |c^T x^k| + |\phi_{[\underline{x}, \bar{x}]}(r^k) + \phi_{[l, u]}(y^k)|) \\ \|Ax^k - \Pi_{[l, u]}(Ax^k)\|_2 &\leq \epsilon(1 + \|Ax^k\|_2) \\ \|c + A^T y^k + r^k\|_2 &\leq \epsilon(1 + \|c\|_2). \end{aligned} \quad (5)$$

Since iteration (3) does not track a reduced cost vector $r^k \in \mathbf{R}^n$, we compute it as $r^k = \Pi_{B_{[\underline{x}, \bar{x}]}}(-c - A^T y^k)$ where $\Pi_{B_{[\underline{x}, \bar{x}]}}$ is the Euclidean projection on the barrier cone of the variable bounds. In the actual implementation, we replace $\Pi_{B_{[\underline{x}, \bar{x}]}}$ with an alternative formulation that tends to be more robust to bounds taking large values, see Appendix A of [Applegate et al. \[2025\]](#).

Infeasibility detection. To detect infeasibility, we apply the conditions recently developed based on the infimal displacement vector of operator splitting algorithms [Pazy \[1971\]](#), [Banjac et al. \[2019\]](#), [Applegate et al. \[2024\]](#), specifically applied to Halpern iterations [Park and Ryu \[2023\]](#). In particular, given the primal-dual iterates x^{k-1}, y^{k-1} and reduced cost r^{k-1} , we apply the operator T obtaining $(\tilde{x}^k, \tilde{y}^k) = T(x^{k-1}, y^{k-1})$ and $\tilde{r}^k = \Pi_{B_{[\underline{x}, \bar{x}]}}(-c - A^T \tilde{y}^k)$. Then, we compute the displacement vectors $\delta x^k = \tilde{x}^k - x^{k-1}$, $\delta y^k = \Pi_{B_{[l, u]}}(\tilde{y}^k - y^{k-1})$, and $\delta r^k = \Pi_{B_{[\underline{x}, \bar{x}]}}(\tilde{r}^k - r^{k-1})$. We define the ϵ -approximate primal infeasibility conditions as

$$\begin{aligned} \phi_{[l, u]}(\delta y^k) + \phi_{[\underline{x}, \bar{x}]}(\delta r^k) &< 0, \\ \|A^T \delta y^k + \delta r^k\| &\leq \epsilon(\phi_{[l, u]}(\delta y^k) + \phi_{[\underline{x}, \bar{x}]}(\delta r^k)). \end{aligned} \quad (6)$$

Similarly, the ϵ -approximate dual infeasibility conditions are

$$\begin{aligned} c^T \delta x^k &< 0, \quad \|\delta x^k - \Pi_{R_{[\underline{x}, \bar{x}]}}(\delta x^k)\| \leq \epsilon |c^T \delta x^k|, \\ \|A \delta x^k - \Pi_{R_{[l, u]}}(A \delta x^k)\| &\leq \epsilon |c^T \delta x^k|, \end{aligned} \quad (7)$$

where $\Pi_{R_{[a, b]}}$ is the Euclidean projection onto the recession cone of hyperrectangle $[a, b]$, which is defined as $R_{[a, b]} = \{v \mid v_i \geq 0 \text{ if } b_i = \infty; v_i \leq 0 \text{ if } l_i = -\infty; v_i = 0 \text{ otherwise}\}$.

5 Solving batches of problems

Instead of solving a single instance of problem (1), we consider solving a *batch* of N instances with the same data matrix A , and with varying problem vectors. We stack the problem vectors in the objective matrix $C = [c^1 \cdots c^N] \in \mathbf{R}^{n \times N}$ and the bounds matrices $\underline{X} = [x^1 \cdots x^N], \bar{X} = [\bar{x}^1 \cdots \bar{x}^N] \in \mathbf{R}^{n \times N}$, $L = [l^1 \cdots l^N]$, and $U = [u^1 \cdots u^N] \in \mathbf{R}^{n \times N}$. By defining the matrices of primal iterates as $X^k = [x_1^k \cdots x_N^k] \in \mathbf{R}^{n \times N}$, dual iterates as $Y^k = [y_1^k \cdots y_N^k] \in \mathbf{R}^{m \times N}$, and combined iterates as $Z^k = [z_1^k \cdots z_N^k] \in \mathbf{R}^{(n+m) \times N}$ we can rewrite iteration (3) as

$$Z^{k+1} = \frac{k+1}{k+2} (2T(Z^k) - Z^k) + \frac{1}{k+2} Z^0, \quad (8)$$

with the operator $T(Z^k) = (X, Y)$ defined componentwise as

$$\begin{cases} X = \Pi_{[\underline{X}, \bar{X}]} (X^k - \tau \otimes (C + A^T Y^k)) \\ Y = Y^k + \sigma \otimes A(2X - X^k) - \sigma \otimes \Pi_{[L, U]}(\sigma^{-1} \otimes Y^k + A(2X - X^k)), \end{cases} \quad (9)$$

and the projection operators representing the elementwise matrix projection. In addition, we have $w, \tau, \sigma \in \mathbf{R}^N$, since we keep a different value for each subproblem. As for the notation of primal weight and step sizes, we define the Kronecker products $\sigma \otimes X := [\sigma_1 x_1, \dots, \sigma_N x_N]$ and $\tau \otimes Y := [\tau_1 y_1, \dots, \tau_N y_N]$, that is, every column of X and Y gets a different step size.

Restarts. To adapt the restarting logic to take care of batches of LPs, we define the *averaged* fixed-point residual metric as $\tilde{r}(Z^k) = (1/N) \sum_{j=1}^N r(z_j^k)$, that is, the average residual of the columns of matrix Z^k , where each residual is computed as in (4), but using the corresponding values of primal weight w_j and step-sizes τ_j and σ_j . Whenever the average residual $\tilde{r}(Z^k)$ satisfies one of the three conditions as the ones for the single-instance residual (4), we restart all the batches at the same time, by recomputing the new primal weights w_j^{n+1} by exponential smoothing, and the step-sizes τ_j^{n+1} and σ_j^{n+1} accordingly, for each problem $j = 1, \dots, N$.

Stopping criteria and infeasibility detection. The stopping conditions for our batched algorithm are as in (5), but rewritten in matrix notation. The same apply to infeasibility criteria (6) and (7). Whenever we finish solving a problem in the batch, we permute the iterate matrices so that the final columns correspond to the solved problems; equivalently, we keep track of $\pi = (\pi_1, \dots, \pi_N)$ as a permutation of the indices, with $X^k = [x_{\pi_1}^k \cdots x_{\pi_N}^k]$ and $Y^k = [y_{\pi_1}^k \cdots y_{\pi_N}^k]$. In this way, we stop updating those variables and reduce the kernel sizes dynamically.

Matrix-matrix products and optimal batch size. The major bottleneck in the batched algorithm are matrix-matrix products $A^T Y$ and AX , which can be significantly accelerated on GPUs. Moreover, observe that the cost of computing AX^k and $A^T Y^k$ is weakly dependent on the batch size (or the number of columns in X^k and Y^k). We varied the batch size and timed 10 matrix-matrix products of AX^0 and 10 matrix-matrix products of $A^T Y^0$ using the constraint matrix A from the MIPLIB benchmark problem `csched007` [Yunes \[2009\]](#). Figure 1 shows the times that CUDA library cuSPARSE takes to compute these matrix-matrix products on a RTX 4500 ADA GPU. Observe that from batch size 32 to 512 the time taken for these products remains constant at approximately 0.03 ms. After a batch size of 512 the time for these products increases with the batch size. We define the optimal batch size as the one that maximizes the number of matrix-vector multiplies per second. The optimal batch size, influenced by factors like the constraint matrix A , GPU, and software configuration, cannot be predetermined. For a given problem and GPU, we estimate it by timing a few matrix-matrix products before solving the MIP.

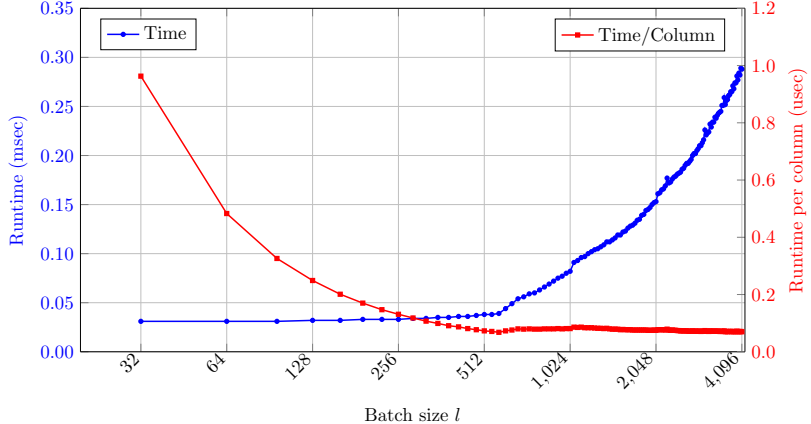


Figure 1: Sparse Matrix-Matrix Multiplies vs Batch Size on `csched007`. Total time for 10 AX and 10 A^TY operations (blue circle markers on the left y-axis) and time/column (red square markers on the right y-axis).

Naive batched implementation. Although the computational speed-ups achievable by matrix-matrix multiplies over batches seem very promising, a naive batched implementation of our algorithm could be very inefficient due to data movement between CPU and GPU, which causes significant memory overhead. In the next section we tailor our batched first-order method to strong branching, a core task in mixed integer programming. In Appendix 5.2, we outline similar customizations to implement optimization-based bound tightening.

5.1 Full strong branching

A key step in branch-and-bound algorithms for MIP is choosing which fractional variable to branch on at each node. Full strong branching (FSB) solves two LPs for each fractional variable: one that rounds up and one that rounds down [Achterberg et al. \[2005\]](#). The resulting objective values determine the branching score.

Precisely, consider an optimal solution x^{rel} of the LP relaxation at the current node with p fractional variables. For notational simplicity, assume the first p components of x^{rel} are fractional. FSB solves $N = 2p$ LPs: for each fractional variable x_i ($i = 1, \dots, p$), we solve one LP with $x_i \geq \lceil x_i^{\text{rel}} \rceil$ (branch up) and one with $x_i \leq \lfloor x_i^{\text{rel}} \rfloor$ (branch down). All N problems share the same cost vector c , constraint bounds l , u , and base variable bounds \underline{x} , \bar{x} ; only one bound component differs per problem.

In matrix notation, the objective and constraint bounds are $C = c\mathbf{1}^T$, $L = l\mathbf{1}^T$, and $U = u\mathbf{1}^T$. The variable bound matrices $\underline{X}, \bar{X} \in \mathbf{R}^{n \times N}$ have columns equal to \underline{x} and \bar{x} , respectively, except

- Column i (branch up on x_i): $(\underline{X})_{ii} = \lceil x_i^{\text{rel}} \rceil$,
- Column $p+i$ (branch down on x_i): $(\bar{X})_{i,p+i} = \lfloor x_i^{\text{rel}} \rfloor$.

Since only one bound entry changes per problem, we avoid forming \underline{X} and \bar{X} explicitly; instead, we index into x^{rel} , \underline{x} , and \bar{x} as needed. Once memory is allocated for p fractional variables, the same allocation serves smaller values of p , which naturally occurs as the tree deepens and more variables become fixed.

5.2 Optimization-based bound tightening

Optimization-based bound tightening (OBBT) is a core preprocessing step in MIP solvers, in which we update the bounds of each variable as $\underline{x}_i = \max\{\underline{x}_i, \underline{x}_i^{\text{obbt}}\}$ and $\bar{x}_i = \min\{\bar{x}_i, \bar{x}_i^{\text{obbt}}\}$, where

$$\begin{aligned} \underline{x}_i^{\text{obbt}} &= \min & \bar{x}_i^{\text{obbt}} &= \max & x_i \\ \text{s.t.} & l \leq Ax \leq u & \text{s.t.} & l \leq Ax \leq u \\ & \underline{x} \leq x \leq \bar{x} & & \underline{x} \leq x \leq \bar{x}, \end{aligned}$$

for $i = 1, \dots, n$. This corresponds to solving $2n = N$ LPs having the same constraint bounds, l, u , and variable bounds \underline{x}, \bar{x} . The objectives correspond to the maximization and minimization of each component of x . In matrix form, this corresponds to matrix bounds $L = l\mathbf{1}^T, U = u\mathbf{1}^T, \underline{X} = \underline{x}\mathbf{1}^T$, and $\bar{X} = \bar{x}\mathbf{1}^T$, all in $\mathbf{R}^{n \times N}$. The objective matrix becomes $C = [I - I] \in \mathbf{R}^{n \times N}$. Similarly to FSB, we never materialize matrix C , where we instead smartly reference its columns that correspond to the canonical basis vectors with alternating signs.

Before ending Section 5, it is important to note that none of the MIP solvers, either commercial or academic, uses FSB or performs OBBT extensively on all variables. A number of work limits are used to maintain the computational footprint of those methods — which are widely acknowledged to be extremely powerful — under control. For strong branching, one selects a restricted candidate subset of variables and the LPs are solved by limiting the number of Simplex pivots. For OBBT, the LPs of some variables are solved (heuristically) once triggered by conditions capturing the likelihood of strengthening the variable bound. In other words, the computational section below aims at answering the question: can one exploit FSB and OBBT at their full strength by moving the associated computation to GPUs with our proposed algorithmic approach?

6 Numerical experiments

In this section, we present our computational results for full strong branching and OBBT using benchmark instances from the literature. Specifically, for both strong branching and OBBT, we evaluate the performance of our batched algorithms described in Sections 5.1 and 5.2, respectively, by solving LPs as if we were at the root node of a branch-and-bound tree.

Implementation details. We implemented the code in standard C++17 and used the CUDA Toolkit and the Thrust library to develop the main GPU kernels. Our implementation does not perform any dynamic memory allocation at runtime. All necessary data is transferred to the GPU before use according to the techniques described in Section 5.

For the matrix operations, we rely on the cuSPARSE and cuBlas libraries. We store in memory both sparse matrices A and A^T , and we use `cusparseSpMM` to compute AX and A^TY , that is, the product between sparse and dense matrices. We use `cublasDgemv` to compute matrix vector operations such as, for instance, X^Tc , which compute $c^T x_i$ for every column x_i of X , and `cublasDnrm2` for vector norms. All other functions are executed on the GPU using our own customized CUDA kernels.

Hardware details. We use a B200 and a H100 on the brev NVIDIA cloud infrastructure mounted on a virtual machine equipped with an Intel Xeon CPU with 56 physical cores and 128 GB of RAM.

6.1 FSB integration within CUOPT MIP solver

We integrate BATCHLP into the branch-and-bound method used in NVIDIA CUOPT 26.02 [NVIDIA \[2025\]](#). CUOPT performs a round of strong branching after solving the root relaxation to initialize pseudocosts for fractional variables. These pseudocosts are then used to make branching decisions. CUOPT’s default strong-branching implementation splits the subproblems evenly across a set of threads. Each thread uses dual simplex, warm-started from the root’s optimal basis, to solve each LP to optimality.

In our main experiments, we use the instances introduced in [Gasse et al. \[2019\]](#) to perform a computational study on learning branching strategies that can be competitive with full strong branching, while being computable in a very short time. Here, we take a different perspective: rather than approximating FSB, we aim to execute it by exploiting the GPU, solving each subproblem LP to optimality as fast as possible with BATCHLP.

Figure 2 summarizes the results; full details are reported in Table 1. Table 1 compares the time required to perform a single round of strong branching using dual simplex on multiple threads (8, 16, 32, and 64 threads on a Dell workstation with 56 physical cores – Intel Xeon CPU) versus BATCHLP. We use the random

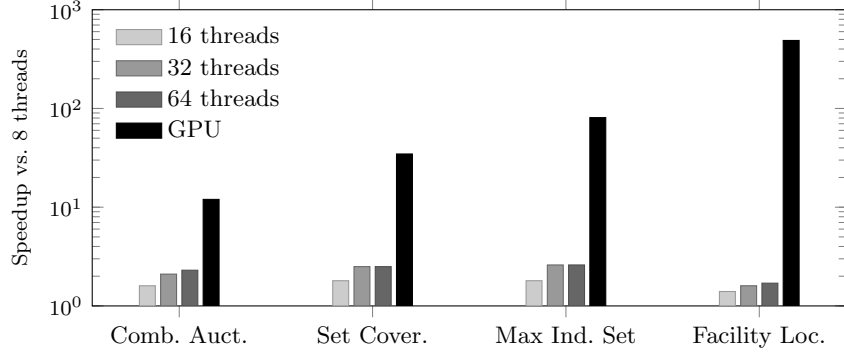


Figure 2: Speedup of FSB runtime vs. 8-thread CPU baseline. GPU achieves 12–489× speedup. Full results in Table 1.

generator from [Gasse et al. \[2019\]](#) to generate instances from four families of combinatorial optimization problems: Combinatorial Auctions, Set Covering, Maximum Independent Set, and Facility Location. Within each family, instances are ordered by increasing size in terms of the number of constraints m , variables n , and nonzeros nnz . The number of subproblems to be solved, denoted by $|S|$, varies across problem classes.

For each family, we report the total speedup relative to the runtime of dual simplex in parallel on 8 threads. The speedup from using more threads is not linear, and the difference between 32 and 64 threads is minimal. In contrast, BATCHLP yields a substantial speedup across all instances (except the smallest one); for the Facility Location MIPs, it achieves a speedup of 488.5×.

6.2 OBBT results

In this section, we use BATCHLP independently of cuOpt and customized to perform OBBT by carefully handling the incumbent best dual bound on the objective value. We compare its performance to an OBBT implementation based on the commercial solver Gurobi. While in strong branching, the lower numerical accuracy of first-order methods is less critical (branching scores are used only as a heuristic to order variables), in OBBT, we must guarantee the use of a *safe* dual bound before restricting the domain of any variable. For this reason, when running OBBT in BATCHLP, we enforce a higher numerical accuracy when checking dual feasibility ($\epsilon_{\text{dual}} = 10^{-8}$), and we subtract/add

$$\Delta = \epsilon \left(1 + |c^T x| + |\phi_{[x, \bar{x}]}(r) + \phi_{[l, u]}(y)| \right),$$

to the lower/upper bounds computed via OBBT. Finally, we update a bound only if the improvement is larger than 10^{-4} .

In the numerical experiments, we apply OBBT to neural network verification instances from [Nair et al. \[2020\]](#). Figure 3 summarizes the results, with full details in Table 2. Table 2 reports our results, comparing BATCHLP with a sequential version of Gurobi. Similarly to Table 1: m is the number of constraints, n is the number of variables, while $|S| = 2n$ is not explicitly reported. Finally, den is the density of the coefficient matrix A (similarly to the nnz value reported in Table 1). For Gurobi dual simplex, we report the total runtime and the average number of pivots required to solve each subproblem to optimality. For BATCHLP, we report the total runtime, the speed-up over the sequential version, and the number of subproblems solved before hitting the iteration limit. The last two columns report the number of variables whose domain changes, and the average domain reduction (as a percentage of the original domain). We remark that, since we perform OBBT on the model obtained after Gurobi MIP presolve, several standard bound-reduction techniques have already been applied to the original model.

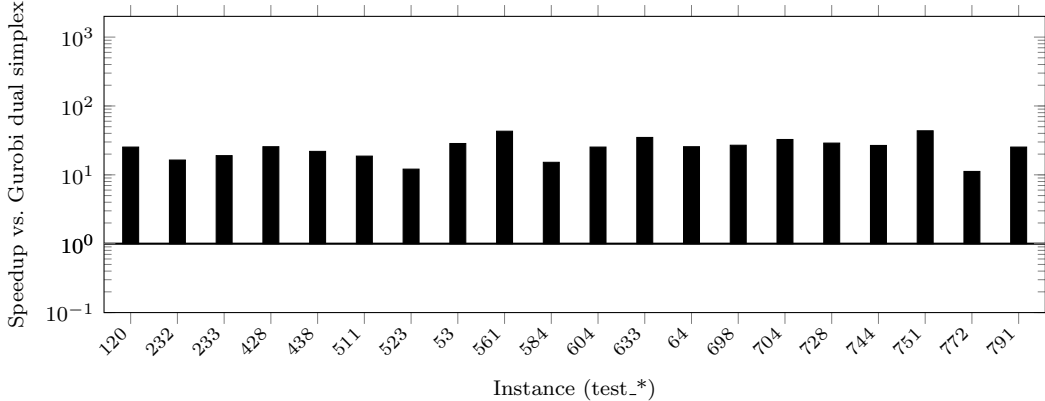


Figure 3: OBBT speedup of BATCHLP vs. Gurobi dual simplex on neural network verification instances. Average speedup: $25.7\times$. Full results in Table 2.

Interpreting the speed-up. The results in Table 2 show a large sped-up (25.7 on average) that is significant considering the quality of the Gurobi simplex implementation. Such an average speed-up of BATCHLP with respect to sequential dual simplex should be interpreted as follows: under ideal CPU parallelism (which we have shown in Table 1 does not happen), solving in parallel the strong branching LPs with dual simplex using 26 threads on 26 physical cores should yield a runtime comparable to that of BATCHLP running on a single GPU.

6.3 Results on MIPLIB 2017

Finally, we present preliminary results on running BATCHLP on MIPLIB 2017 using the default strong-branching strategy we implemented in cuOpt 26.02, i.e., running the dual simplex in parallel, with a limit of only 200 pivots per subproblem. Figure 4 summarizes the results; full details are reported in Table 3 in the Appendix. Table 3 reports results for a subset of instances on which BATCHLP on an H100 GPU is competitive with the dual simplex running in parallel on 28 threads (i.e., 28 physical cores). Unsurprisingly, for all other MIPLIB 2017 instances not reported in the table, the dual simplex on 28 threads (with the 200-pivot limit) is faster than BATCHLP.

Although the impact of moving strong branching to the GPU has been presented only on few MIP instances and within a solver that is admittedly less developed than the commercial ones like Gurobi, it is important to note that the integration of such GPU mechanism within a state-of-the-art solver is a standalone research question that deserves specific work beyond the scope of the current paper. Initial tests with cuOpt 26.02 on a family of ‘qap’ instances (see instance qap10 in Table 3) where we run the entire branch and bound using either BATCHLP or the default parallel simplex implementation show very promising results but they are too preliminary to be reported in full.

7 Conclusions

In this paper, we introduced a batched first-order method for solving multiple linear programs in parallel on GPUs, specifically focusing on mixed-integer programming (MIP) challenges like strong branching and optimization-based bound tightening. Our approach extends the primal-dual hybrid gradient algorithm, leveraging matrix-matrix operations to fully exploit the capabilities of modern GPU architectures. Through a series of computational experiments, we demonstrated significant speed-ups over traditional simplex-based methods, particularly in instances with large problem sizes and numerous subproblems in the batches. This advancement offers the MIP community a powerful tool for handling repeated subproblem solutions more

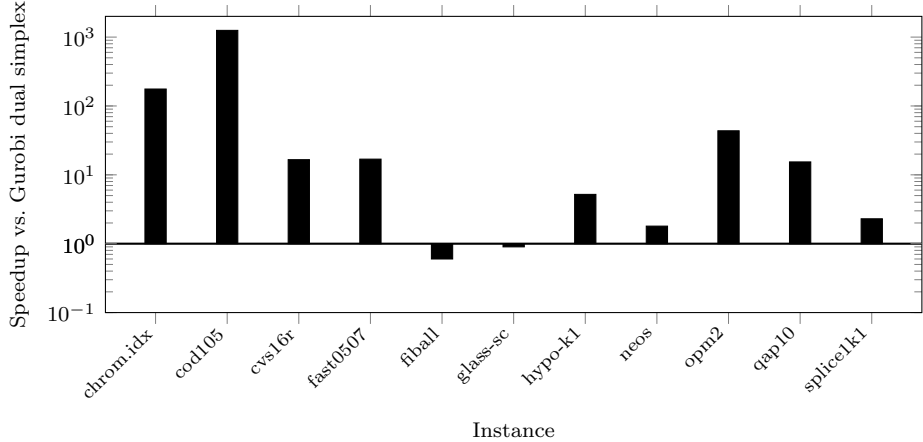


Figure 4: MIPLIB 2017 speedup of BATCHLP vs. cuOpt dual simplex (28 threads). Values below 1 indicate dual simplex is faster. Full results in Table 3.

efficiently, paving the way for fully incorporating GPUs in MIP algorithms.

Acknowledgments

Bartolomeo Stellato is supported by the NSF CAREER Award ECCS-2239771 and the ONR YIP Award N000142512147. Stefano Gualandi acknowledges the contribution of the National Recovery and Resilience Plan, Mission 4 Component 2-Investment 1.4-National Center for HPC, Big Data and Quantum Computing (project code: CN_00000013), funded by the European Union-NextGenerationEU. The authors are thankful for NVIDIA for providing credits to access **brev** cloud infrastructure with DGX B200 GPUs.

References

- T. Achterberg, T. Koch, and A. Martin. Branching rules revisited. *Operations Research Letters*, 33(1):42–54, 2005.
- A. Agrawal, B. Amos, S. Barratt, S. Boyd, S. Diamond, and Z. Kolter. Differentiable convex optimization layers. In *Advances in Neural Information Processing Systems*, 2019.
- D. Applegate, M. Díaz, O. Hinder, H. Lu, M. Lubin, B. O’Donoghue, and W. Schudy. Practical large-scale linear programming using primal-dual hybrid gradient. *Advances in Neural Information Processing Systems*, 34:20243–20257, 2021.
- D. Applegate, O. Hinder, H. Lu, and M. Lubin. Faster first-order primal-dual methods for linear programming using restarts and sharpness. *Mathematical Programming*, 201(1):133–184, 2023.
- D. Applegate, M. Díaz, H. Lu, and M. Lubin. Infeasibility detection with primal-dual hybrid gradient for large-scale linear programming. *SIAM Journal on Optimization*, 34(1):459–484, 2024.
- D. Applegate, M. Díaz, O. Hinder, H. Lu, M. Lubin, B. O’Donoghue, and W. Schudy. PDLP: A practical first-order method for large-scale linear programming, 2025. URL <https://arxiv.org/abs/2501.07018>.
- G. Banjac, P. Goulart, B. Stellato, and S. Boyd. Infeasibility detection in the alternating direction method of multipliers for convex optimization. *Journal of Optimization Theory and Applications*, 183:490–519, 2019.

T. Berthold, M. Francobaldi, and G. Hendel. Learning to use cuts. *Mathematical Programming Computation*, 17:437–450, 2025.

M. Besançon, J. Dias Garcia, B. Legat, and A. Sharma. Flexible differentiable optimization via model transformations. *INFORMS Journal on Computing*, 36(2):456–478, 2023.

P. Bonami, A. Lodi, and G. Zarpellon. A classifier to decide on the linearization of mixed-integer quadratic problems in CPLEX. *Operations Research*, 70(6):3303–3320, 2022.

A. Chambolle and T. Pock. A first-order primal-dual algorithm for convex problems with applications to imaging. *Journal of mathematical imaging and vision*, 40(1):120–145, 2011.

A. Chambolle, C. Delplancke, M. Ehrhardt, C.-B. Schönlieb, and J. Tang. Stochastic primal–dual hybrid gradient algorithm with adaptive step sizes. *Journal of Mathematical Imaging and Vision*, 66:294–313, 2024.

K. Chen, D. Sun, Y. Yuan, G. Zhang, and X. Zhao. HPR-LP: An implementation of an HPR method for solving linear programming. *Mathematical Programming Computation*, 2025.

M. Gasse, D. Chételat, N. Ferroni, L. Charlin, and A. Lodi. Exact combinatorial optimization with graph convolutional neural networks. *Advances in Neural Information Processing Systems*, 32, 2019.

P. Gupta, M. Gasse, E. Khalil, P. Mudigonda, A. Lodi, and Y. Bengio. Hybrid models for learning to branch. *Advances in Neural Information Processing Systems*, 33:18087–18097, 2020.

B. Halpern. Fixed points of nonexpanding maps. *Bulletin of the American Mathematical Society*, 73(6):957–961, 1967.

T. Liu and H. Lu. A new crossover algorithm for lp inspired by the spiral dynamic of PDHG. *arXiv preprint arXiv:2409.14715*, 2024.

H. Lu and J. Yang. Restarted Halpern PDHG for linear programming. *arXiv preprint arXiv:2407.16144*, 2024.

H. Lu and J. Yang. cuPDLP.jl: A GPU implementation of restarted primal-dual hybrid gradient for linear programming in Julia. *Operations Research*, 73(6):3440–3452, 2025.

H. Lu, Z. Peng, and J. Yang. MPAX: Mathematical programming in JAX. *arXiv preprint arXiv:2412.09734*, 2024.

H. Lu, Z. Peng, and J. Yang. cuPDLPx: A further enhanced gpu-based first-order solver for linear programming, 2025. URL <https://arxiv.org/abs/2507.14051>.

V. Nair, S. Bartunov, F. Gimeno, I. Von Glehn, P. Lichocki, I. Lobov, B. O’Donoghue, N. Sonnerat, C. Tjandraatmadja, P. Wang, et al. Solving mixed integer programs using neural networks. *arXiv preprint arXiv:2012.13349*, 2020.

NVIDIA. cuOpt. <https://github.com/NVIDIA/cuopt>, 2025. Accessed: January 30, 2026.

B. O’Donoghue. Operator splitting for a homogeneous embedding of the linear complementarity problem. *SIAM Journal on Optimization*, 31(3):1999–2023, 2021.

B. O’Donoghue, E. Chu, N. Parikh, and S. Boyd. Conic optimization via operator splitting and homogeneous self-dual embedding. *Journal of Optimization Theory and Applications*, 169(3):1042–1068, 2016.

J. Park and E. K. Ryu. Accelerated infeasibility detection of constrained optimization and fixed-point iterations. In A. Krause, E. Brunskill, K. Cho, B. Engelhardt, S. Sabato, and J. Scarlett, editors, *Proceedings of the 40th International Conference on Machine Learning*, volume 202 of *Proceedings of Machine Learning Research*, pages 27294–27345. PMLR, 23–29 Jul 2023. URL <https://proceedings.mlr.press/v202/park23k.html>.

A. Pazy. Asymptotic behavior of contractions in hilbert space. *Israel Journal of Mathematics*, 9(2):235–240, 1971.

E. Rothberg. New options for solving giant LPs. Gurobi Webinar, December 2024. URL <https://www.gurobi.com/events/new-options-for-solving-giant-lps/>.

L. Scavuzzo, K. Aardal, A. Lodi, and N. Yorke-Smith. Machine learning augmented branch and bound for mixed integer linear programming. *Mathematical Programming*, pages 1–44, 2024.

M. Schubiger, G. Banjac, and J. Lygeros. GPU acceleration of ADMM for large-scale quadratic programming. *Journal of Parallel and Distributed Computing*, 144:55–67, 2020.

B. Stellato, G. Banjac, P. Goulart, A. Bemporad, and S. Boyd. OSQP: An operator splitting solver for quadratic programs. *Mathematical Programming Computation*, 12(4):637–672, 2020.

Z. Xiong and R. M. Freund. The role of level-set geometry on the performance of PDHG for conic linear optimization. *arXiv preprint arXiv:2406.01942*, 2024.

T. Yunes. CuSPLIB 1.0: A library of single-machine cumulative scheduling problems, 2009. <http://moya.bus.miami.edu/tallys/cusplib/>.

Table 1: Runtime (in seconds) comparison of dual simplex and BATCHLP as implemented in cuOpt 26.02.

Instance	Problem				cuOpt 26.02 – Dual Simplex				BATCHLP GPU B200
	<i>m</i>	<i>n</i>	<i>nnz</i>	<i>S</i>	8 threads	16 threads	32 threads	64 threads	
Combinatorial Auctions									
inst_100_1500	360	1399	8418	154	0.03	0.02	0.02	0.03	0.05
inst_300_1500	557	1453	8547	512	0.60	0.41	0.26	0.27	0.09
inst_300_3000	857	2840	16635	514	0.73	0.48	0.31	0.36	0.08
inst_500_1500	755	1466	7989	800	2.24	1.42	1.04	0.97	0.20
inst_500_3000	1025	2867	16493	846	2.51	1.51	1.24	1.04	0.09
Total runtime				6.11	3.84	2.87	2.67	0.51	
Speed-up				1.0	1.6	2.1	2.3	12.0	
Set Covering									
inst_1000r_1000c_0.01	1000	1000	10000	330	1.15	0.63	0.47	0.49	0.11
inst_1000r_1000c_0.05	1000	1000	50000	136	0.44	0.27	0.19	0.20	0.06
inst_1000r_2000c_0.01	1000	2000	20000	309	1.22	0.72	0.50	0.51	0.10
inst_1000r_2000c_0.05	1000	2000	100000	116	0.31	0.20	0.15	0.18	0.06
inst_1000r_3000c_0.01	1000	3000	30000	265	0.77	0.54	0.37	0.37	0.09
inst_1000r_3000c_0.05	1000	3000	150000	127	0.59	0.35	0.24	0.27	0.07
inst_2000r_1000c_0.01	1978	999	19781	382	2.58	1.81	1.18	1.18	0.12
inst_2000r_1000c_0.05	2000	1000	100000	182	1.96	1.06	0.79	0.76	0.07
inst_2000r_2000c_0.01	2000	2000	40000	449	5.96	4.16	2.69	2.57	0.15
inst_2000r_2000c_0.05	2000	2000	200000	170	1.73	1.00	0.73	0.76	0.08
inst_3000r_1000c_0.01	3000	1000	30000	493	8.71	5.31	3.69	3.51	0.15
inst_3000r_1000c_0.05	3000	1000	150000	164	1.67	0.98	0.77	0.72	0.07
inst_3000r_3000c_0.01	3000	3000	90000	522	17.60	8.56	6.21	5.93	0.17
inst_3000r_3000c_0.05	3000	3000	450000	191	4.14	2.25	1.82	1.78	0.11
Total runtime				48.83	27.84	19.80	19.23	1.41	
Speed-up				1.0	1.8	2.5	2.5	34.6	
Maximum Independent Set									
inst_1000_12	8060	1000	18815	1888	47.71	22.91	17.69	17.20	0.29
inst_1000_4	8012	1000	18770	1882	62.79	31.74	24.24	23.38	0.28
inst_1000_8	8209	1000	18982	1870	63.23	32.43	22.56	21.33	0.29
inst_2000_12	18992	2000	41213	3320	88.56	52.97	34.86	35.01	0.87
inst_2000_4	18832	2000	40960	3320	65.39	35.53	27.00	26.16	0.83
inst_2000_8	18961	2000	41100	3328	77.92	40.23	29.28	29.09	0.84
inst_3000_12	35612	3000	71338	5226	115.12	63.56	43.92	45.12	2.02
inst_3000_4	35582	3000	71289	5218	130.66	71.48	52.26	52.57	1.99
inst_3000_8	35604	3000	71325	5204	105.64	69.68	42.99	43.46	1.96
Total runtime				757.02	420.53	294.80	293.32	9.37	
Speed-up				1.0	1.8	2.6	2.6	80.8	
Facility Location									
inst_1200_200_10	241401	240200	960400	92	410.71	283.56	247.59	215.15	0.41
inst_1200_200_15	241401	240200	960400	88	192.56	117.60	96.49	100.83	0.40
inst_1200_200_5	241401	240200	960400	62	135.40	110.95	88.99	81.05	0.38
inst_400_200_10	80601	80200	320400	40	22.52	18.09	18.05	17.97	0.12
inst_400_200_15	80601	80200	320400	26	24.68	16.73	19.17	17.42	0.11
inst_400_200_5	80601	80200	320400	32	4.84	4.97	5.64	5.05	0.11
inst_800_200_10	161001	160200	640400	58	132.33	93.22	81.69	85.90	0.24
inst_800_200_15	161001	160200	640400	60	108.64	76.74	69.47	65.15	0.22
inst_800_200_5	161001	160200	640400	32	33.22	23.98	30.13	24.30	0.19
Total runtime				1064.90	745.84	657.22	612.82	2.18	
Speed-up				1.0	1.4	1.6	1.7	488.5	

A OBBT Results

Table 2 presents detailed results for the OBBT experiments discussed in Section 6.

Table 2: Results for OBBT applied after MIP presolve of Gurobi: Dual Simplex–Gurobi 13.0 on Intel Xeon Platinum 8592; BATChLP iteration limit 100 000 (always hit) on a GPU B200 (cost of machine 5.29 USD/hour).

Instance	m	n	den	Dual simplex		BATChLP			var changed	
				runtime	pivots	runtime	Speed-up	solved	num	perc.
test_120	1564	1767	1.8%	507.9	755.9	20.1	25.3	3429/3534	141	4.0%
test_232	1296	1491	2.0%	271.2	594.1	16.6	16.4	2866/2982	105	3.5%
test_233	1315	1512	1.9%	225.8	495.6	11.9	19.0	2973/3024	110	3.6%
test_428	1485	1617	2.0%	551.7	887.6	21.6	25.6	2859/3234	93	2.9%
test_438	1229	1332	2.3%	263.7	660.7	12.0	21.9	2591/2664	112	4.2%
test_511	1100	1208	2.8%	250.8	734.4	13.4	18.7	1800/2416	168	7.0%
test_523	932	1036	3.1%	145.0	622.4	11.9	12.1	1981/2072	134	6.5%
test_53	1635	1741	1.6%	485.3	760.3	17.1	28.5	3287/3482	108	3.1%
test_561	1457	1643	2.0%	573.8	902.9	13.4	43.0	3167/3286	134	4.1%
test_584	883	980	3.2%	141.2	666.9	9.3	15.2	1922/1960	117	6.0%
test_604	1362	1529	2.1%	385.5	719.3	15.3	25.3	2730/3058	59	1.9%
test_633	1453	1614	1.9%	462.0	786.2	13.2	34.9	3119/3228	150	4.7%
test_64	1589	1736	1.7%	503.6	766.2	19.7	25.6	3290/3472	108	3.1%
test_698	1347	1494	2.0%	309.5	665.9	11.5	26.9	2915/2988	115	3.9%
test_704	1574	1731	1.7%	513.5	769.3	15.7	32.6	3369/3462	129	3.7%
test_728	1410	1570	2.0%	393.1	710.2	13.6	28.9	3004/3140	121	3.9%
test_744	1575	1801	1.6%	435.6	662.8	16.3	26.7	3513/3602	124	3.4%
test_751	1672	1927	1.6%	613.6	784.3	14.1	43.6	3751/3854	132	3.4%
test_772	907	973	3.2%	128.9	633.0	11.5	11.2	1572/1946	99	5.1%
test_791	1410	1548	2.1%	432.0	773.0	17.1	25.3	2899/3096	100	3.2%
mean				379.7		14.8	25.7		4.1%	

B MIPLIB 2017 Results

Table 3 presents detailed results for the MIPLIB 2017 experiments discussed in Section 6.

Table 3: Comparison of cuOpt dual simplex running on 28 threads (28 physical cores) with BATCHLP running on a GPU H100.

Instance	m	n	nnz	$ S $	Dual simplex	BATCHLP	Speed-up
chromaticindex512-7	33791	36864	135156	51604	3522.4	20.0	176.2
cod105	1024	1024	57344	256	212.8	0.2	1251.7
cvs16r128-89	4633	3472	12528	6420	20.9	1.3	16.6
fast0507	482	62171	401756	556	5.8	0.3	16.9
fiball	2387	32899	101452	518	22.8	37.1	0.6
glass-sc	6119	214	63918	202	1.0	1.1	0.9
hypothyroid-k1	5189	2595	431326	4806	3292.7	627.9	5.2
neos-5052403-cygnet	19134	27593	2448853	1272	63.7	35.8	1.8
opm2-z10-s4	146325	5958	340288	11170	1921.5	44.1	43.6
qap10	1820	4150	18200	2442	28.8	1.9	15.4
splice1k1	6504	3252	1758012	3816	3355.3	1468.6	2.3